SCIENCE CHINA
Information Sciences

• RESEARCH PAPER •

August 2022, Vol. 65 182401:1–182401:10
https://doi.org/10.1007/s11432-021-3350-9

Experimental demonstration of photonic spike-timing-dependent plasticity based on a VCSOA

Ziwei SONG[1], Shuiying XIANG[1,2*], Xingyu CAO[1], Shihao ZHAO[1] & Yue HAO[2]

[1]*State Key Laboratory of Integrated Service Networks, Xidian University, Xi'an* 710071*, China;*
[2]*State Key Discipline Laboratory of Wide Bandgap Semiconductor Technology, School of Microelectronics, Xidian University, Xi'an* 710071*, China*

Received 29 April 2021/Revised 20 August 2021/Accepted 18 October 2021/Published online 29 June 2022

Abstract We experimentally design two photonic spike-timing-dependent plasticity (STDP) schemes based on a single vertical-cavity semiconductor optical amplifier (VCSOA) and demonstrate the photonic implementation of STDP characteristics. In the first scheme, a single-polarized optical pulse train is injected into the VCSOA, in which a pair of optical pulses with a time difference is designed to emulate the pre-synaptic and post-synaptic spikes. In the second scheme, dual-polarized optical pulses emulating the pre-synaptic and post-synaptic spikes are injected into the single VCSOA. Furthermore, the effects of the initial wavelength detuning and the power of the input optical pulse on the STDP curve are analyzed. The proposed photonic STDP schemes based on a single VCSOA need relatively low bias current and power consumption, and thus, are ideal optical synaptic devices forming key components in the construction of the photonic neuromorphic computing system.

Keywords neuromorphic photonics, vertical-cavity semiconductor optical amplifier, spike-timing-dependent plasticity, optical neural systems, pulsed optical injection

Citation Song Z W, Xiang S Y, Cao X Y, et al. Experimental demonstration of photonic spike-timing-dependent plasticity based on a VCSOA. Sci China Inf Sci, 2022, 65(8): 182401, https://doi.org/10.1007/s11432-021-3350-9

1 Introduction

The human brain offers extremely energy-efficient information processing performance with ultralow power consumption in carrying out complicated tasks. Many researchers have made great efforts in exploring the functional and structural advantages of the brain and designing brain-inspired neuromorphic computing systems [1–3] by mimicking both the structure and working mechanism of the biological neural system. In recent years, neuromorphic computing platforms [4–15] made up of artificial spiking neurons and synapses have a promising prospect as the emergence and development of spiking neural networks (SNNs) [16, 17] in electronic and photonic fields. In particular, neuromorphic photonic approaches [8–15], which overcome the limitations of energy-efficiency and operation speed that occurs in electronic approaches [18], have attracted considerable attention. They exhibit the advantages of ultrafast performance, large bandwidth, low cross talk, and high parallelism.

The human brain is composed of around 100 billion highly interconnected neurons transmitting information between each other by the way of firing spikes. The connection between neurons is called the synapse, which plays an important role in performing complex information processing and cognitive computing functions [19]. The connection strength between two neurons, i.e., the synaptic weight, can be modulated by neural spikes from the pre-synaptic neuron (PRE) and post-synaptic neuron (POST). The modulation of synaptic weights called synaptic plasticity forms an important foundation of learning and memory in the neural circuits. The spike-timing-dependent plasticity (STDP) [20, 21] is considered a fundamental synaptic plasticity mechanism in a biological neural system, which uses the relative timing of pre-synaptic and post-synaptic spikes to update the synaptic weight.

* Corresponding author (email: jxxsy@126.com)

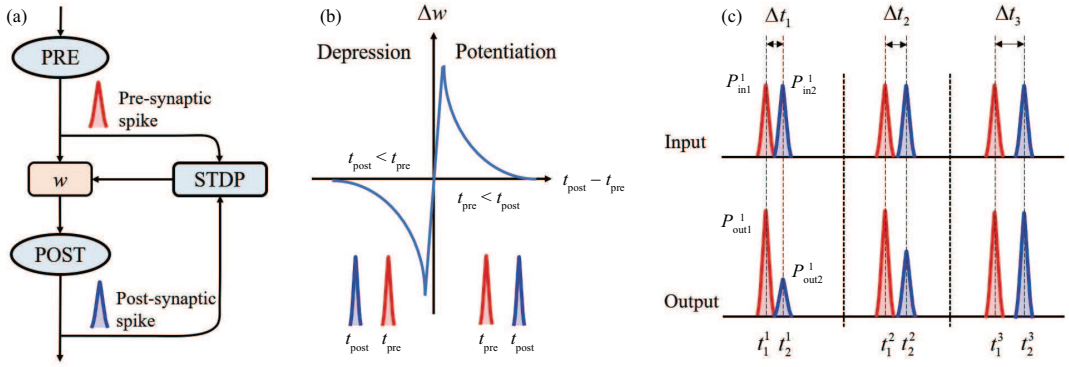

Figure 1 (Color online) (a) The basic schematics of synaptic learning in neurons; (b) the potentiation and depression windows of the STDP curve; (c) three pairs of input optical pulses and corresponding output pulses with different time differences.

In neuromorphic computing systems, it is significant to develop an ideal synaptic device mimicking biological STDP characteristics. To date, various photonic devices have successfully emulated the STDP learning rule of biological synapses by experimental study or numerical simulations [22–26]. For instance, the research group of Fok et al. [22] reported for the first time the experimental implementation of the optical STDP based on a semiconductor optical amplifier (SOA) and an electro-absorption modulator (EAM). Besides, they also experimentally demonstrated the implementation of photonic STDP utilizing a single SOA and investigated the application of a photonic STDP module in supervised and unsupervised learning schemes [23,24]. Ren et al. [25] proposed an optical STDP scheme using two SOAs and achieved a weight-dependent learning window and reward-based reinforcement learning by introducing the feedback control of SOA current-injection. In 2016, Li et al. [26] experimentally achieved an antisymmetric STDP learning rule and antisymmetric anti-STDP learning rule based on the cross-gain modulation (XGM) within a single SOA.

In our previous studies [27–29], we numerically achieved photonic STDP by using a vertical-cavity surface-emitting laser (VCSEL) operating below the threshold as a vertical-cavity semiconductor optical amplifier (VCSOA) [30–32] for the first time and presented a computational model for the photonic STDP with low power consumption. However, the experimental demonstration of photonic STDP based on a single VCSOA has not been reported. In this paper, the demonstration of the photonic implementation of STDP characteristics is presented by experiments. Herein, we design two photonic experimental schemes based on a single VCSOA under single-polarized and dual-polarized pulsed optical injections, respectively. Furthermore, we also explore the effects of some controllable parameters on the STDP characteristics.

The rest of this paper is organized as follows. The principle for the implementation of photonic STDP based on a single VCSOA is presented in Section 2. In Section 3, we demonstrate the photonic STDP scheme based on a single VCSOA subject to a single-polarized pulsed optical injection. And the effects of initial wavelength detuning, bias current, and injection power on the STDP curve are explored. In Section 4, we further propose a photonic STDP scheme based on a VCSOA subject to dual-polarized pulsed optical injections, and analyze the effect of the initial wavelength detuning. At last, the conclusion is drawn in Section 5.

2 Principle

In biological neural systems, a neuron (PRE) generates pre-synaptic spikes (fire time $t_{\rm pre}$) that propagate along the axon and are transmitted through a synapse to the next neuron (POST) that generates the post-synaptic action spikes (fire time $t_{\rm post}$). The basic schematics of synaptic learning in neurons are shown in Figure 1(a). Here, the change of synaptic weight follows the STDP rule which includes two learning windows illustrated in Figure 1(b). In the potentiation window, the synaptic weight is strengthened when a pre-synaptic spike precedes a post-synaptic spike ($t_{\rm pre} < t_{\rm post}$). Otherwise, the synaptic weight is weakened when a pre-synaptic spike follows a post-synaptic spike ($t_{\rm post} < t_{\rm pre}$) resulting in the depression window.

In the proposed photonic STDP circuits, a VCSOA is a key device and the effect of XGM within a single VCSOA plays an important role in the realization of the STDP learning curve. Hence, Figure 1(c)

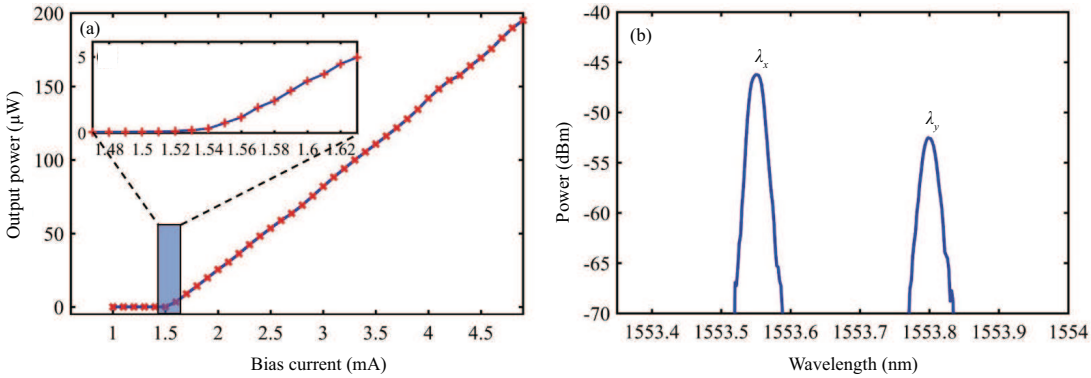

Figure 2 (Color online) (a) The output power as a function of the applied bias current (P-I curve) of the 1500 nm-VCSEL. (b) The optical spectra of the VCSEL operating at 1.42 mA. λ_x (λ_y) denotes the peak wavelength of the orthogonal (parallel) polarization mode of VCSEL.

shows the gain property of VCSOA subject to pulsed optical injections [27]. Here, three pairs of input optical pulses and the corresponding output pulses with different time differences are presented. For convenience, we define the first (second) pulse of each pair of optical pulses as the control (signal) pulse. Here, P^i_{in1} (P^i_{in2}) and t^i_1 (t^i_2) denote optical power and peak location of the control (signal) pulse of the i-th pair of input optical pulses, respectively. Accordingly, P^i_{out1} (P^i_{out2}) denotes output optical power of the i-th control (signal) pulse, and $\Delta t_i = t^i_2 - t^i_1$ denotes the time difference between the control and signal pulses of the i-th pair. When two optical pulses with Δt_i are injected into the VCSOA, the lagged signal pulse experiences a different gains due to the carrier depletion in the VCSOA induced by the leading control pulse. That is to say, the signal pulse experiences XGM while the control pulse experiences no XGM. As we can see that the smaller the time difference ($\Delta t_1 < \Delta t_2 < \Delta t_3$) is, the lower the power of the lagged output pulse ($P^1_{\text{out2}} < P^2_{\text{out2}} < P^3_{\text{out2}}$) is. Therefore, the STDP curve can be obtained by adjusting Δt_i.

In the following experiments, a commercially available VCSEL (SEOUL VIOSYS) with an emission wavelength at 1550 nm operating below the threshold current serves as a VCSOA. Figure 2(a) plots the output power as a function of applied bias current (P-I curve) of the VCSEL measured at room temperature (293 K). As shown in the inset of Figure 2(a), the threshold current is $I_{\text{th}} = 1.52$ mA. The optical spectra of the VCSEL operating at 1.42 mA are shown in Figure 2(b). The VCSEL has two coexisting orthogonally-polarized modes, in which the peak wavelength of the orthogonal polarization (XP) mode is $\lambda_x = 1553.550$ nm and the peak wavelength of the parallel polarization (YP) mode is $\lambda_y = 1553.798$ nm.

3 The experimental scheme with a VCSOA subject to a single-polarized pulsed optical injection

The experimental setup of the proposed photonic STDP scheme based on a single VCSOA subject to a single-polarized pulsed optical injection is illustrated in Figure 3(a). In this experiment, a continuous wave optical signal is generated by a tunable laser (TL) and modulated through a modulator (Mod). An arbitrary waveform generator (AWG, Tektronix AWG70001A) is used to produce the different pulse patterns. Here, a pair of optical pulses with a given time difference is designed to emulate the pre-synaptic and post-synaptic spikes. Then, the modulated optical signal experiences the VCSOA's gain amplification to obtain the output optical pulse signal. Specifically, the TL emission is passed through an isolator (ISO) which can avoid undesired reflections. A variable optical attenuator (VOA) and polarization controller (PC1) are used to control the input power and polarization of the optical signal, respectively. The PC2 is used to adjust the polarization state of the modulated optical signal. Then, the modulated light is divided into two paths via a 50:50 optical fiber coupler (OC1). The first optical path is connected to a power meter (PM) to monitor the injected power. The second optical path injects the modulated optical signal into the VCSOA through an optical circulator (CIRC). Then, the output of VCSOA is collected by the CIRC and analyzed with a photodetector (PD, Agilent HP11982A), an oscilloscope (SCOPE, Keysight DSOV334A), and an optical spectrum analyzer (OSA, Advantest Q8384). Here, the distributed feedback laser (DFB) is used as the TL source, and the generated optical signal is injected into the XP

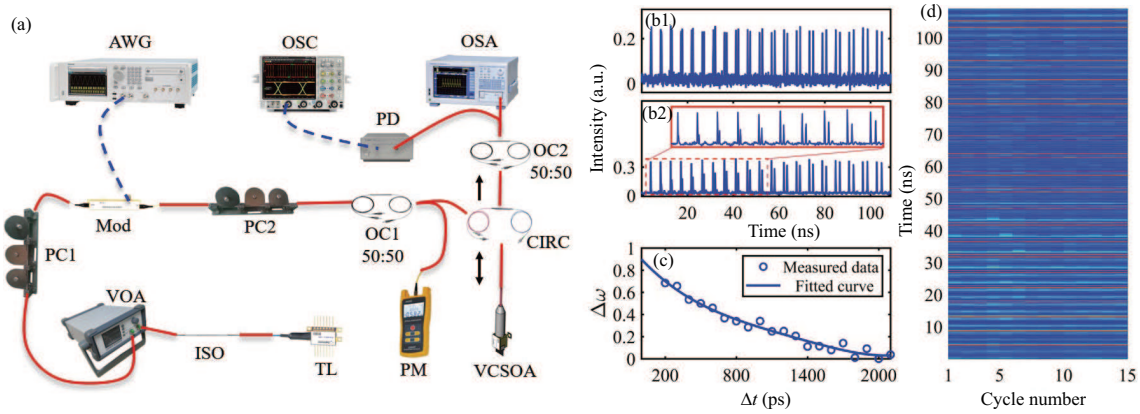

Figure 3 (Color online) (a) Experimental setup of photonic STDP based on a single VCSOA subject to a single-polarized pulsed optical injection. Optical fiber connections are shown in solid red lines and electrical connections in dashed blue lines. (b1) The modulated input pulse train which is injected into the VCSOA. (b2) The output pulse train corresponding to the input pulse train. The inset is the enlarged time series of the first 10 pairs of output pulses. (c) The potentiation window of the photonic STDP. The blue empty circles are the calculated data according to experimental measurement. The blue line is the fitted curve based on the blue empty circles. (d) The temporal map of superimposed time series shows the response of VCSOA to the arrival of 15 consecutive input pulse trains.

mode of VCSOA. Hence, the initial wavelength detuning is defined as $\Delta\lambda = \lambda_p - \lambda_x$, in which λ_p is the peak wavelength of the DFB laser.

Based on this experimental setup, the STDP characteristics can be observed and the corresponding STDP curve can be calculated. The experimental measured results are shown in Figures 3(b1) and (b2), in which $\Delta\lambda = 0.04$ nm. Figure 3(b1) presents the modulated input pulse train injected into the VCSOA including 20 consecutive pulse pairs with the same optical power and different time differences. Here, the values of Δt for 20 consecutive pulse pairs vary from 200 to 2100 ps. Figure 3(b2) shows the corresponding output pulse train of the VCSOA, and the inset is the enlarged time series of the first 10 pairs of output pulses. Obviously, with the increase of time difference Δt, the output power of the lagged signal pulse increases gradually. The experimental results agree well with the numerical simulation results reported in our previous work [27]. Hence, it is verified that the proposed scheme can emulate the STDP function. For clarity, we only present the time series of the first 10 pairs of output pulses in the following study.

According to the computational model for the photonic STDP presented in our numerically simulation work [27] and the measured data of Figure 3(b2), the STDP curve $\Delta\omega(\Delta t)$ can be calculated from the output channel of VCSOA by

$$\Delta\omega(\Delta t) = (P_{2\max} - \max[P_{\text{out2}}(t)])/P_{2\max}, \tag{1}$$

where $P_{2\max}$ is the maximum peak power of the output pulse, and $\max[P_{\text{out2}}(t)]$ is the peak power of the output pulse for a given Δt. $\Delta P(\Delta t) = P_{2\max} - \max[P_{\text{out2}}(t)]$, which is the loss of output power at a given Δt, corresponds to the magnitude of weight update of the STDP potentiation window. As shown in Figure 3(c), the blue empty circles are the calculated $\Delta\omega$ for giving Δt by using (1). And the blue line is the fitted curve based on the blue empty circles, which corresponds to the potentiation window of the photonic STDP. The experimental result is similar to the biological experiment, but at a much faster time scale. Moreover, it coincides with the numerical simulation result based on the VCSOA in terms of operating conditions and time scale. Besides, it is found that the width of the window of the measured photonic STDP based on a VCSOA is much wider than that of previous photonic STDP based on a conventional in-plane SOA (about a few hundred picoseconds). Moreover, in previously photonic STDP circuits based on the SOA, the operating current of SOA is usually large, i.e., several tens of or hundreds of mA [22–24, 26]. But, in our experiments, the operating current of VCSOA is only a few mA. Therefore, our proposed experimental scheme requires much lower bias current and input power, which is desired for low power consumption photonic neuromorphic computing systems.

Additionally, to verify the reproducibility of experimental results, Figure 3(d) shows the temporal map of superimposed time series. Here, we can observe the response of VCSOA to the arrival of 15 identical input pulse trains, in which, the input pulse train is the same as that shown in Figure 3(b1). The color coding in the map indicates increasing intensity from blue to red. Red and yellow correspond to

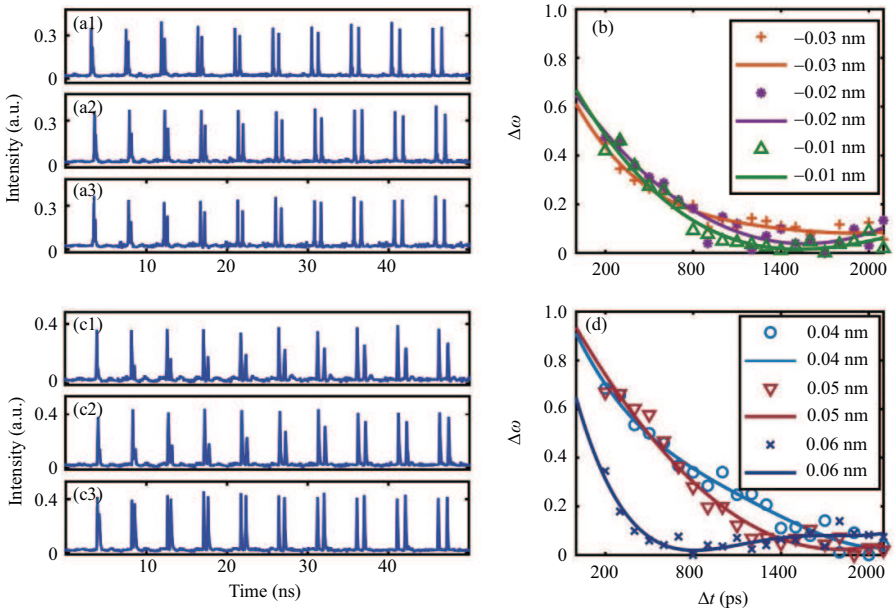

Figure 4 (Color online) (a1)–(a3) The first 10 pairs of output pulse trains corresponding to the input pulse train of Figure 2(b1) under $\Delta\lambda = -0.03$ nm (a1), $\Delta\lambda = -0.02$ nm (a2), $\Delta\lambda = -0.01$ nm (a3). (b) The computed STDP curves corresponding to (a1)–(a3). (c1)–(c3) Output pulse trains corresponding to the input pulse train in Figure 2(b1) under $\Delta\lambda = 0.04$ nm (c1), $\Delta\lambda = 0.05$ nm (c2), $\Delta\lambda = 0.06$ nm (c3). (d) The computed STDP curves corresponding to (c1)–(c3).

high-intensity spikes, while blue and darker blue indicate low background noise. Note, red indicates a higher peak intensity than yellow. The result clearly shows the reproducibility of the output pulse train corresponding to identical input pulse trains, which proves the repeatability of the proposed photonic STDP scheme.

Considering the existence of the peak resonant wavelength of VCSOA, we analyze the effect of initial wavelength detuning $\Delta\lambda$ on the STDP curve. In this experiment, $\Delta\lambda$ is adjusted by controlling the wavelength of the input optical pulse λ_p. Figures 4(a1)–(a3) show the output pulse trains corresponding to the input pulse train of Figure 3(b1) under $\Delta\lambda = -0.03, -0.02, -0.01$ nm, respectively. And Figure 4(b) plots the computed STDP curves according to Figures 4(a1)–(a3). It can be observed that, for different negative $\Delta\lambda$, the obtained STDP curves have almost the same height and width of windows. Similarly, as shown in Figures 4(c1)–(c3) and (d), the output pulse trains and the computed STDP curves under the positive $\Delta\lambda$ are presented. Here, the values of wavelength detuning are $\Delta\lambda = 0.04, 0.05, 0.06$ nm, respectively. It is found that, as the increase of the positive $\Delta\lambda$, the height and width of STDP windows are gradually decreased. Consequently, these results reveal that the STDP curve can be controlled by the initial wavelength detuning experimentally.

Next, we explore the influence of the power of the input optical pulse signal. In the experiment, the input optical power is adjusted by adjusting the VOA. Here, the initial wavelength detuning remains constant, i.e., $\Delta\lambda = 0.04$ nm. From Figures 5(a1)–(a5), the attenuation of input optical power controlled by VOA is 0, 1, 2, 3, 4 dB, respectively. Accordingly, the power of the output optical pulse signal gradually decreases. As we can see, for all cases, the time series of lagged signal pulse output power exhibit STDP characteristics. Figure 5(b) presents the fitted STDP curves corresponding to Figure 5(a). The results show that a small input power leads to a decrease in the height and width of the STDP curves. Hence, the STDP curves can be achieved and adapted by slightly adjusting the power of the input optical pulse signal.

Furthermore, it is necessary to consider the case that the input power of the control pulse is different from that of the signal pulse. Here, the case of different powers is shown by the ratio of the control pulse power to the signal pulse power. As illustrated in Figures 6(a1) and (b1), the input power ratios are 3:1 and 1:3, respectively. And the corresponding output pulse trains are shown in Figures 6(a2) and (b2). We can see that the preceding control pulse pulses always obtain constant gain. But the lagged signal pulses experience different gains due to the carrier depletion caused by the leading control pulses. Similar to the prior experiment results, the time series of signal pulse output power show STDP characteristics. That is to say, the STDP curves can be obtained thanks to the gradually increased gain of the lagged

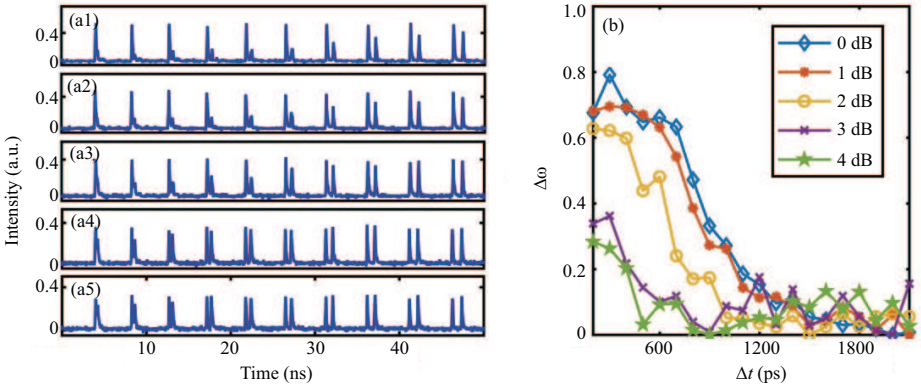

Figure 5 (Color online) (a1)–(a5) Output pulse trains under the input optical power attenuation of 0 dB (a1), 1 dB (a2), 2 dB (a3), 3 dB (a4), 4 dB (a5) with $\Delta\lambda = 0.04$ nm. (b) The computed STDP curves corresponding to (a1)–(a5).

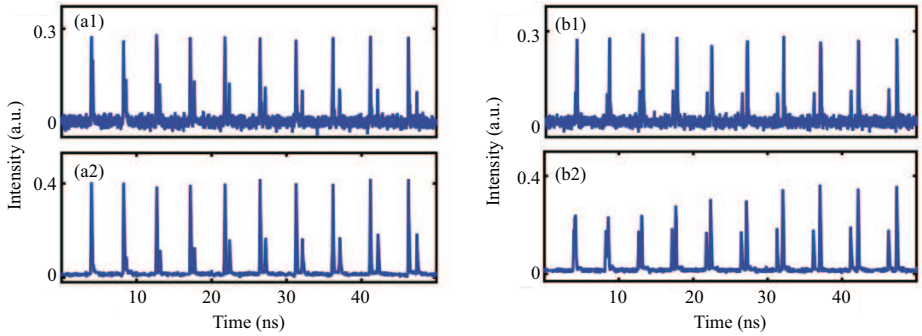

Figure 6 (Color online) (a1) and (b1) Input pulse trains with the power ratio are 3:1 (a1) and 1:3 (b1). (a2) and (b2) Output pulse trains corresponding to the input pulse trains.

signal pulses with the increased Δt.

4 The experimental scheme with a VCSOA subject to dual-polarized pulsed optical injections

In the previous scheme, the pre-synaptic and post-synaptic pulses pairs are included in a single-polarized optical pulse injection, which results in only one output spike train. It can be successfully used to calculate the STDP curve, but the pre-synaptic and post-synaptic spikes cannot be observed and calculated separately. In this section, we propose a scheme that dual-polarized optical pulses emulating the pre-synaptic and post-synaptic spikes are injected into two polarization modes of VCSOA, respectively.

As shown in Figure 7, the experimental setup includes optical spike trains generation and optical STDP circuit. Lights from two DFB lasers at wavelength $\lambda_{\rm pre}$ (DFB1) and $\lambda_{\rm post}$ (DFB2) are respectively modulated by Mod1 and Mod2 driven by an AWG (Tektronix AWG70002B) which outputs two electric signals. And the generated pre-synaptic and post-synaptic optical spike trains are combined by a 50:50 OC as inputs for the optical STDP circuit. Here, VOA1 and VOA2 can tune the power of pre-synaptic and post-synaptic spikes to control the ratio of injection. PCs are used to align the polarization of optical injection, in which the injections of DFB1 and DFB2 are respectively aligned to the XP and YP modes of VCSOA. The corresponding initial wavelength detuning is $\Delta\lambda_{\rm pre} = \lambda_{\rm pre} - \lambda_x$ and $\Delta\lambda_{\rm post} = \lambda_{\rm post} - \lambda_y$. In the optical STDP circuit, an erbium-doped fiber amplifier (EDFA) is used to amplify the total injection power. An optical CIRC is included to redirect the external optical injections to the VCSOA as well as to collect its output light. The polarization beam splitter (PBS) can separate the two orthogonal polarizations of VCSOA. Hence, the output of the VCSOA can be divided into two channel's outputs. Two PDs transform output optical signals into electric signals. The laser diode controllers (LDCs) can control the temperature and current of DFBs and VCSOA to tune the wavelength and output power.

To obtain the optical STDP curve, the injections from two DFBs are carefully set with the help of AWG. The pre-synaptic and post-synaptic spike trains generated from the optical spike trains generation

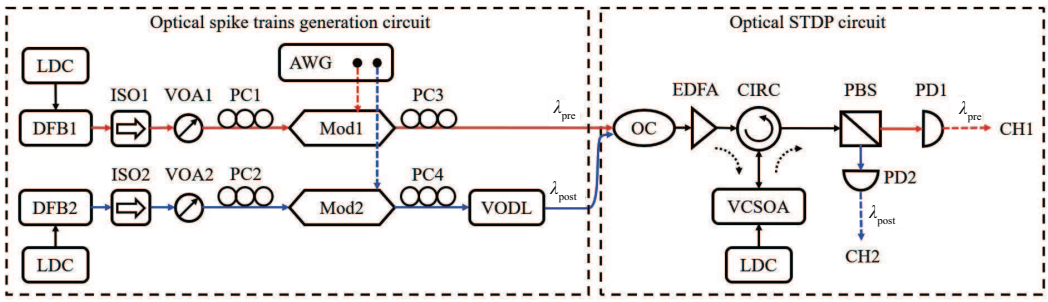

Figure 7 (Color online) Experimental setup of photonic STDP based on a single VCSOA subject to dual-polarized pulsed optical injection. The left part is the optical spike trains generation circuit, and the right part is the optical STDP circuit.

circuit are shown in Figures 8(a1) and (b1). Here, two spike trains both include 65 spikes of which the width is $\sim$ 100 ps. And the periods of the pre-synaptic and post-synaptic spike train are designed to $T_{\rm pre} = 3$ ns and $T_{\rm pre} = 3.05$ ns, respectively. The timings of middle spikes for two trains keep consistent. Thus, the time difference ($\Delta t = t_{\rm post} - t_{\rm pre}$) between pre-synaptic and post-synaptic spike pair increases from -1600 to 1600 ps with an incremental interval of 50 ps. The output spike trains of VCSOA are shown in Figures 8(c1) and (d1). The spike trains in two grey boxes are enlarged and shown in Figures 8(a2)–(d2) and (a3)–(d3). Figures 8(a2)–(d2) plot input and output spike pairs with $\Delta t = -200$ ps and $\Delta t = -150$ ps. And Figures 8(a3)–(d3) plot input and output spike pairs with $\Delta t = 400$ ps and $\Delta t = 450$ ps.

Figure 8(c1) represents channel 1's output (CH1) at $\lambda_{\rm pre}$, Figure 8(d1) represents channel 2's output (CH2) at $\lambda_{\rm post}$, and Figure 8(e) shows the resulted STDP curve according to two channels' power levels. When $\Delta t < 0$ ($t_{\rm pre} > t_{\rm post}$), as shown on the left side of Figure 8(c1), the lagging pre-synaptic spike experiences XGM because the preceding post-synaptic spike induces gain depletion. The output of CH1 decreases when the $|\Delta t|$ decreases, and the peak power for a given Δt is defined by $\max[P_{\rm out1}(t)]$. As shown on the left side of Figure 8(d1), the preceding post-synaptic spike is amplified without the influence of VCSOA's gain depletion, so the output of CH2 is almost constant. Here, we compute the mean value of peak power as the constant peak power which is defined by $P_{\rm 2max}$. When $\Delta t > 0$ ($t_{\rm pre} < t_{\rm post}$), as shown on the right side of Figure 8(c1), the preceding pre-synaptic spike experiences no XGM. The output of CH1 is almost constant and the mean peak power is denoted as $P_{\rm 1max}$. However, the lagging post-synaptic spike experiences the gain depletion of VCSOA, and the output power increases with the increasing $|\Delta t|$, as shown on the right side of Figure 8(d1). So, the peak power for a given Δt is defined by $\max[P_{\rm out2}(t)]$. Therefore, the loss of the output power $\Delta P = P_{\rm 2max} - \max[P_{\rm out2}(t)]$ ($\Delta P = \max[P_{\rm out1}(t)] - P_{\rm 1max}$) determines the magnitude of weight increase (decrease) of the STDP potentiation (depression) window. Referring to our prior numerically simulation work [27], the STDP curve $\Delta\omega(\Delta t)$ can be calculated from two output channels by

$$\Delta\omega(\Delta t) = \begin{cases} (P_{\rm 2max} - \max[P_{\rm out2}(t)])/P_{\rm 2max}, & \Delta t > 0, \\ (\max[P_{\rm out1}(t)] - P_{\rm 1max})/P_{\rm 1max}, & \Delta t < 0, \\ 0, & \Delta t = 0. \end{cases} \tag{2}$$

The calculated STDP curve is shown in Figure 8(e).

As we all know, there are four ideal STDP Hebbian learning rules [33], including asymmetric/symmetric STDP Hebbian learning rules and asymmetric/symmetric anti-STDP Hebbian learning rules. The asymmetric STDP Hebbian learning curve is calculated by (2) and shown in Figure 8(e). Besides, the other three STDP Hebbian learning rules can be obtained by changing the calculation method [26]. The asymmetric anti-STDP Hebbian learning curve can be calculated by

$$\Delta\omega(\Delta t)_{\rm asymmetric\ anti\text{-}STDP} = \begin{cases} (\max[P_{\rm out2}(t)] - P_{\rm 2max})/P_{\rm 2max}, & \Delta t > 0, \\ (P_{\rm 1max} - \max[P_{\rm out1}(t)])/P_{\rm 1max}, & \Delta t < 0, \\ 0, & \Delta t = 0. \end{cases} \tag{3}$$

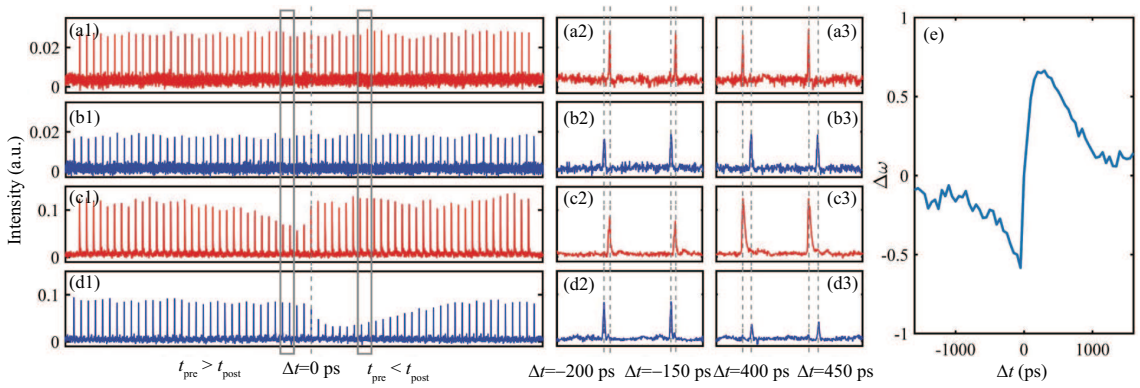

Figure 8 (Color online) (a1) The generated pre-synaptic spike train at $\lambda_{\rm pre}$. (b1) The generated post-synaptic spike train at $\lambda_{\rm post}$. (c1) The CH1 spike train at $\lambda_{\rm pre}$. (c2) The CH2 spike train at $\lambda_{\rm post}$. (a2), (b2), (c2), (d2) The enlarged spike trains corresponding to the left grey box. (a3), (b3), (c3), (d3) The enlarged spike trains corresponding to the right grey box. (e) The resulted STDP curve according to two channels' power levels.

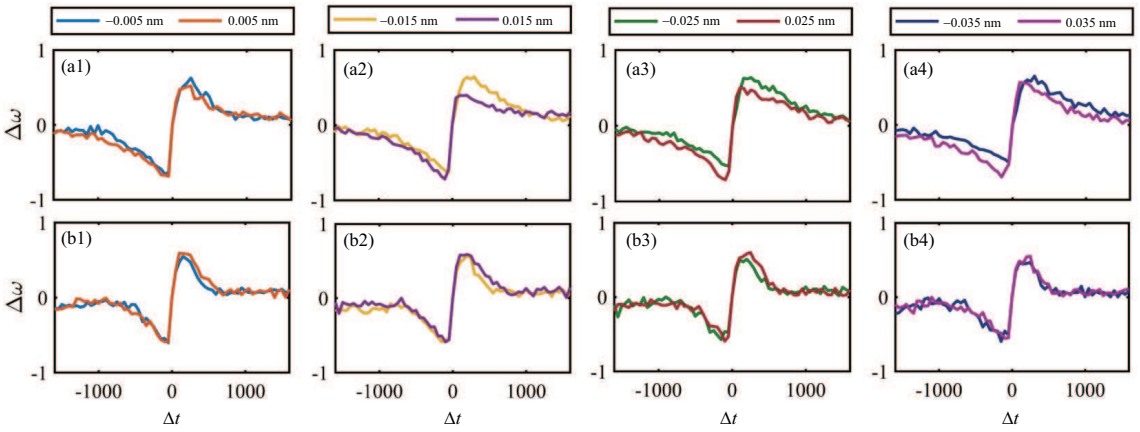

Figure 9 (Color online) (a1)–(a4) The calculated STDP curves for $\Delta\lambda_{\rm pre} = \pm 0.005$ nm (a1), $\Delta\lambda_{\rm pre} = \pm 0.015$ nm (a2), $\Delta\lambda_{\rm pre} = \pm 0.025$ nm (a3), $\Delta\lambda_{\rm pre} = \pm 0.035$ nm (a4) with $\Delta\lambda_{\rm post} = 0.035$ nm. (b1)–(b4) The calculated STDP curves for $\Delta\lambda_{\rm post} = \pm 0.005$ nm (b1), $\Delta\lambda_{\rm post} = \pm 0.015$ nm (b2), $\Delta\lambda_{\rm post} = \pm 0.025$ nm (b3), $\Delta\lambda_{\rm post} = \pm 0.035$ nm (b4) with $\Delta\lambda_{\rm pre} = 0.005$ nm.

The symmetric STDP Hebbian learning curve can be calculated by

$$\Delta\omega(\Delta t)_{\text{symmetric STDP}} = \begin{cases} (\max[P_{\rm out2}(t)] - P_{\rm 2max})/P_{\rm 2max}, & \Delta t \geqslant 0, \\ (\max[P_{\rm out1}(t)] - P_{\rm 1max})/P_{\rm 1max}, & \Delta t < 0. \end{cases} \tag{4}$$

The symmetric anti-STDP Hebbian learning curve can be calculated by

$$\Delta\omega(\Delta t)_{\text{symmetric anti-STDP}} = \begin{cases} (P_{\rm 2max} - \max[P_{\rm out2}(t)])/P_{\rm 2max}, & \Delta t \geqslant 0, \\ (P_{\rm 1max} - \max[P_{\rm out1}(t)])/P_{\rm 1max}, & \Delta t < 0. \end{cases} \tag{5}$$

Next, we investigate the effect of initial wavelength detuning on the STDP curves. On the one hand, Figures 9(a1)–(a4) present the calculated STDP curves for different $\Delta\lambda_{\rm pre}$ under $\Delta\lambda_{\rm post} = 0.035$ nm. The results show that, for the potentiation window, the width and height of the STDP window for the negative case are slightly larger than the positive case. However, for the depression window, the opposite trend is observed. On the other hand, the STDP curves for different $\Delta\lambda_{\rm post}$ are shown in Figures 9(b1)–(b4), in which $\Delta\lambda_{\rm pre}$ is fixed at 0.005 nm. It can be seen that the STDP curve for the negative case is almost the same as the positive case. Hence, tunable STDP curves can be achieved by simply adjusting the detuning $\Delta\lambda_{\rm pre}$ and $\Delta\lambda_{\rm post}$.

5 Conclusion

In summary, we firstly proposed a photonic STDP scheme based on a single VCSOA subject to a single-polarized pulsed optical injection and experimentally demonstrated the photonic implementation of the

STDP function. The reproducibility of this proposed STDP scheme is verified by analyzing the response of VCSOA to the arrival of several identical input pulse trains. Besides, we experimentally demonstrated that the height and width of the STDP window could be controlled by adjusting either the initial wavelength detuning or the power of the input optical pulse signal. And the STDP curve still can be obtained when the powers of two input optical pulses are different. To observe and analyze output pre-synaptic and post-synaptic spikes separately, we further proposed a scheme based on a single VCSOA subject to dual-polarized pulsed optical injections. The STDP curve is obtained by calculating two channel output spike trains. And the height and width of SDTP windows can be adjusted by changing initial wavelength detuning. Note that, with the advancement of photonic integrated circuits, such proposed optical STDP schemes may be integrated into a photonic chip, which may improve the footprint efficiency.

Compared with previous optical STDP circuits using conventional SOAs, relatively lower current and power consumption are required and a wider window (about a few thousand picoseconds) can be obtained for the two proposed photonic STDP schemes based on a single VCSOA. Note that, there is a certain difference between the two schemes. In the first scheme, the output spike train of VCSOA can be directly used to observe STDP characteristics, but the post-processing for calculating the STDP curve is relatively more complicated. However, in the second scheme, the output train of VCSOA is separated into two outputs corresponding to two input spike trains, which allows more intuitive observation of STDP characteristics. Notably, the fine adjustment of PBS is required to implement separation.

The proposed photonic STDP schemes can be employed for the online learning of STDP-based unsupervised and supervised learning algorithms, and thus, have potential applications in pattern recognition, rapid sensory processing, fast autonomous systems, high-performance scientific computing, and machine learning tasks.

Acknowledgements This work was supported in part by National Natural Science Foundation of China (Grant Nos. 61974177, 61674119), National Outstanding Youth Science Fund Project of National Natural Science Foundation of China (Grant No. 62022062), Fundamental Research Funds for the Central Universities (Grant No. JB210114), and Fundamental Research Funds for the Central Universities and the Innovation Fund of Xidian University (Grant No. 5001-20109215456). The authors would like to thank Tektronix Inc. for providing the arbitrary waveform generators (AWG70001A, AWG70002B).

References

1 Nawrocki R A, Voyles R M, Shaheen S E. A mini review of neuromorphic architectures and implementations. IEEE Trans Electron Devices, 2016, 63: 3819–3829
2 Schuman C D, Potok T E, Patton R M, et al. A survey of neuromorphic computing and neural networks in hardware. 2017. ArXiv:1705.06963
3 Roy K, Jaiswal A, Panda P. Towards spike-based machine intelligence with neuromorphic computing. Nature, 2019, 575: 607–617
4 Painkras E, Plana L A, Garside J, et al. SpiNNaker: a 1-W 18-core system-on-chip for massively-parallel neural network simulation. IEEE J Solid-State Circ, 2013, 48: 1943–1953
5 Benjamin B V, Gao P, McQuinn E, et al. Neurogrid: a mixed-analog-digital multichip system for large-scale neural simulations. Proc IEEE, 2014, 102: 699–716
6 Davies M, Srinivasa N, Lin T H, et al. Loihi: a neuromorphic manycore processor with on-chip learning. IEEE Micro, 2018, 38: 82–99
7 Pei J, Deng L, Song S, et al. Towards artificial general intelligence with hybrid Tianjic chip architecture. Nature, 2019, 572: 106–111
8 Shen Y, Harris N C, Skirlo S, et al. Deep learning with coherent nanophotonic circuits. Nat Photon, 2017, 11: 441–446
9 Feldmann J, Youngblood N, Wright C D, et al. All-optical spiking neurosynaptic networks with self-learning capabilities. Nature, 2019, 569: 208–214
10 Xiang S Y, Ren Z X, Zhang Y H, et al. All-optical neuromorphic XOR operation with inhibitory dynamics of a single photonic spiking neuron based on a VCSEL-SA. Opt Lett, 2020, 45: 1104–1107
11 Song Z W, Xiang S Y, Ren Z X, et al. Spike sequence learning in a photonic spiking neural network consisting of VCSELs-SA with supervised training. IEEE J Sel Top Quantum Electron, 2020, 26: 1–9
12 Xiang S Y, Ren Z X, Song Z W, et al. Computing primitive of fully VCSEL-based all-optical spiking neural network for supervised learning and pattern classification. IEEE Trans Neural Netw Learn Syst, 2021, 32: 2494–2505
13 Robertson J, Hejda M, Bueno J, et al. Ultrafast optical integration and pattern classification for neuromorphic photonics based on spiking VCSEL neurons. Sci Rep, 2020, 10: 6098
14 Robertson J, Wade E, Kopp Y, et al. Toward neuromorphic photonic networks of ultrafast spiking laser neurons. IEEE J Sel Top Quantum Electron, 2020, 26: 1–15
15 Xiang S Y, Han Y N, Song Z W, et al. A review: photonics devices, architectures, and algorithms for optical neural computing. J Semicond, 2021, 42: 023105
16 Maass W. Networks of spiking neurons: the third generation of neural network models. Neural Networks, 1997, 10: 1659–1671
17 Ghosh-Dastidar S, Adeli H. Spiking neural networks. Int J Neur Syst, 2009, 19: 295–308
18 Merolla P A, Arthur J V, Alvarez-Icaza R, et al. A million spiking-neuron integrated circuit with a scalable communication network and interface. Science, 2014, 345: 668–673
19 Ho V M, Lee J A, Martin K C. The cell biology of synaptic plasticity. Science, 2011, 334: 623–628
20 Bi G Q, Poo M M. Synaptic modifications in cultured hippocampal neurons: dependence on spike timing, synaptic strength, and postsynaptic cell type. J Neurosci, 1998, 18: 10464–10472

21 Bi G Q, Poo M M. Synaptic modification by correlated activity: Hebb's postulate revisited. Annu Rev Neurosci, 2001, 24: 139–166

22 Fok M P, Tian Y, Rosenbluth D, et al. Pulse lead/lag timing detection for adaptive feedback and control based on optical spike-timing-dependent plasticity. Opt Lett, 2013, 38: 419–421

23 Toole R, Fok M P. Photonic implementation of a neuronal algorithm applicable towards angle of arrival detection and localization. Opt Express, 2015, 23: 16133–16141

24 Toole R, Tait A N, de Lima T F, et al. Photonic implementation of spike-timing-dependent plasticity and learning algorithms of biological neural systems. J Lightwave Technol, 2016, 34: 470–476

25 Ren Q S, Zhang Y L, Wang R, et al. Optical spike-timing-dependent plasticity with weight-dependent learning window and reward modulation. Opt Express, 2015, 23: 25247–25258

26 Li Q, Wang Z, Le Y S, et al. Optical implementation of neural learning algorithms based on cross-gain modulation in a semiconductor optical amplifier. In: Proceedings of SPIE, 2016. 10019

27 Xiang S Y, Gong J K, Zhang Y H, et al. Numerical implementation of wavelength-dependent photonic spike timing dependent plasticity based on VCSOA. IEEE J Quantum Electron, 2018, 54: 1–7

28 Xiang S Y, Zhang Y N, Gong J K, et al. STDP-based unsupervised spike pattern learning in a photonic spiking neural network with VCSELs and VCSOAs. IEEE J Sel Top Quantum Electron, 2019, 25: 1–9

29 Xiang S Y, Han Y N, Guo X X, et al. Real-time optical spike-timing dependent plasticity in a single VCSEL with dual-polarized pulsed optical injection. Sci China Inf Sci, 2020, 63: 160405

30 Hurtado A, Gonzalez-Marcos A, Henning I D, et al. Optical bistability and nonlinear gain in 1.55 μm VCSOA. Electron Lett, 2006, 42: 483–484

31 Hurtado A, Henning I D, Adams M J. Effects of parallel and orthogonal polarization on nonlinear optical characteristics of a 1550 nm VCSOA. Opt Express, 2007, 15: 9084–9089

32 Hurtado A, Adams M J. Two-wavelength switching with 1550 nm semiconductor laser amplifiers. J Opt Netw, 2007, 6: 434–441

33 Hebb D O. The Organisation of Behaviour: A Neuropsychological Theory. New York: Science Editions, 1949